Vol. 581: 103–117, 2017
https://doi.org/10.3354/meps12313

MARINE ECOLOGY PROGRESS SERIES
Mar Ecol Prog Ser

Published October 13

Enhanced sea surface temperature due to kelp canopies

Yongsheng Wu[1,*], Charles G. Hannah[2], Brian Petrie[1], Xiaoyi Wang[1], Emmanuel Devred[1]

[1]Marine Ecosystem Section, Ocean Ecosystem Sciences Division, Fisheries and Oceans Canada, Bedford Institute of Oceanography, Dartmouth, Nova Scotia B2Y 4A2, Canada

[2]State of the Ocean Section, Ocean Sciences Division, Fisheries and Oceans Canada, Institute of Ocean Sciences, Sidney, British Columbia V8L 4B2, Canada

ABSTRACT: The presence of kelp canopies in the surface oceanic layer modifies the vertical distribution of solar radiation in the water column and thus the sea surface temperature (SST). We examined the modification of SST due to kelp using observational data and a 1-D mixed layer model. The observational data included SST and the normalized difference vegetation index (NDVI), derived from Landsat 8 images from 2013 and 2014. Data analysis showed that SST in kelp forests is consistently higher than that in the ambient kelp-free waters and that the magnitude of SST increases with the increasing mean NDVI with a median value of (mean ± SD) +2.7 ± 1.4°C and a maximum asymptotic value of +5.4°C for an NDVI of 0.80. Using the mixed layer model, the effect of kelp on the vertical attenuation of solar radiation was simulated with an extinction depth derived from published field data. The model successfully captured the observed trend of increasing SST with NDVI. Analysis of the model result indicated that the increased absorption of solar heat caused by kelp changes the distribution of solar heating in the water column which enhances SST but leaves deeper temperatures relatively unaffected. Increased SST leads to a shallower upper mixed layer depth (MLD) and enhances the heat flux from ocean to atmosphere. However, SST in kelp areas may significantly drop below values in kelp-free waters due to strong vertical mixing events. Our study emphasizes the importance of kelp beds in regulating heat flux in coastal areas. While the model in this preliminary study captured some of the dynamics, the scatter of the SST observations for all NDVI values remains problematic. More *in situ* data — kelp concentrations, ocean current, and mixing strengths — and contemporaneous observations of NDVI would be valuable to determine if the scatter of SST about the empirical fit and model predictions could be reduced.

KEY WORDS: Solar radiation · Extinction depth · Surface heating · Mixed layer model · Heat flux · Landsat · Remote sensing

INTRODUCTION

Kelp beds are commonly distributed throughout temperate coastal waters (Dayton 1985). Typically, they grow from rocky substrates and extend upward to the sea surface, where kelp fronds spread out to form dense canopies (Jackson & Winant 1983). Kelp beds serve as food and refuge for a variety of benthic and pelagic animals (Gaylord et al. 2007, Gruber & Kemp 2010). They provide a unique 3-D habitat for marine organisms and are recognized as a vital component of marine ecosystems (Mann 1973).

Studies have indicated that kelp beds modify local ocean current fields by significantly enhancing the physical drag on flows (Jackson & Winant 1983, Gaylord et al. 2007, Rosman et al. 2007). Based on obser-

*Corresponding author: Yongsheng.Wu@dfo-mpo.gc.ca

vations across a kelp forest at Point Loma California (USA), Jackson & Winant (1983) reported that flow speeds in the interior of the forest decreased by as much as 80% compared to those in ambient kelp-free areas; flow speeds along the forest edge, in contrast, increased by up to 20%. The reduction of currents in the interiors of kelp forests enhances the residence time of water there; on the other hand, the increase in flow along the edges enhances the velocity shear between forests and the surrounding waters (Jackson & Winant 1983, Gaylord et al. 2002, 2012, Fram et al. 2008, Gruber & Kemp 2010, Pinsky et al. 2013). Using a 3-D numerical model, Wu et al. (2017) investigated dispersion properties around the kelp beds in Hecate Strait, British Columbia, Canada. They found that the presence of kelp decreased the dispersion rate in the interior of the beds but increased the dispersion rate along bed edges.

In addition to the modifications of flow speeds, the presence of canopies also reduces the penetration of solar radiation, much like trees shade terrestrial vegetation (Gerard 1984, Reed & Foster 1984, Jackson 1987). Using field observations, Gerard (1984) reported that kelp canopies were able to trap 95% of the solar irradiance within the uppermost 1 m. Not surprisingly, one direct effect of the strong shading is to decrease the rate of carbon fixation by kelp tissues below the surface canopies and thus to limit the recruitment and growth of understory algae (Arkema et al. 2009, Gruber & Kemp 2010). Many field studies have documented profound effects of the light reduction by canopies on the underlying benthic community and on biological mechanisms (Gerard 1984, Reed & Foster 1984, Arkema et al. 2009, Gruber & Kemp 2010). Since kelp canopies are able to modify the distribution of solar radiation in the upper surface layer, sea surface temperatures (SSTs) will differ from those in adjacent kelp-free waters.

There is a general agreement that micro-pigments of phytoplankton absorb solar radiation and heat ambient water (Sathyendranath et al. 1991, Nakamoto et al. 2000, Shell et al. 2003, Wu et al. 2007, Chen et al. 2015, Son & Wang 2015). Using satellite images of the ocean color in the Arabian Sea to quantify chlorophyll concentrations and a 1-D upper ocean mixed layer model, Sathyendranath et al. (1991) estimated that biologically induced heating over 1 month could increase the surface water temperature up to ~4°C above the case when chlorophyll levels were not considered. Wu et al. (2007) examined the effect of phytoplankton on SST in the Labrador Sea with a 3-D ocean model and spectrally dependent attenuation coefficients; they found that the bio-optical heating associated with the seasonal change in chlorophyll distribution increased surface layer temperatures by 1 to 3°C. While a number of studies have addressed the effect of micro-pigments on SST, heating due to kelp canopies (macro-pigments) on ocean temperature has not been investigated extensively in the scientific literature. One possible reason is the small spatial scale of kelp coverage, generally extending only several hundred meters offshore in coastal areas, which most ocean-color sensors, such as the Moderate Resolution Imaging Spectroradiometer (MODIS), are not able to resolve given their coarse footprint of 1 km for the thermal bands at nadir. In the present study, we used satellite images with a resolution of 30 m from the Landsat 8 sensor and a mixed layer model to examine the effect of kelp canopies on SST. The study area was in the nearshore waters around 3 groups of islands in the Hecate Strait (Fig. 1), where kelp beds are distributed from depths of 5 to 30 m (Druehl 1978, Lobban 1978, ASL Environmental Sciences 2014).

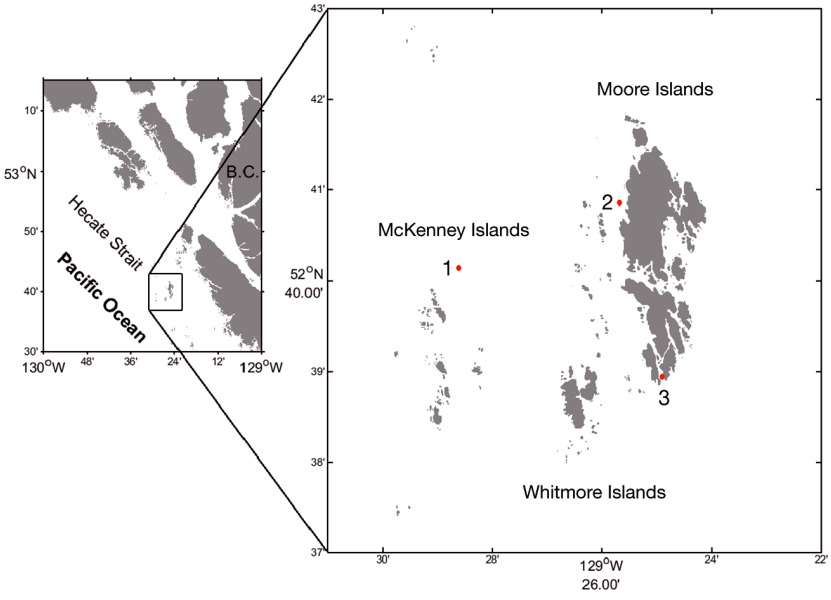

Fig. 1. Study domain, covering near-shore waters around 3 island groups: McKenney, Whitmore, and Moore Islands. Red dots (Sites 1–3) indicate locations where climatological temperatures and salinity were available for model initiation (Foreman et al. 2008). Inset shows the location of the islands in the Hectate Strait off British Columbia (BC), Canada

MATERIALS AND METHODS

Satellite data

We used 2 geophysical products, namely kelp density and SST, derived from Landsat 8 Operational Land Imager and Thermal Infrared Sensor (TIRS) downloaded from the United States Geological Survey (USGS, http://glovis.usgs.gov). The spatial resolution of these images is 30 m. Landsat 8 has a revisit time of about 10 d at the latitude of interest (~50° N). Given the typically cloudy conditions of the region, only 4 clear scenes were available for spring (April–June) and 5 for summer (July–September) for 2013–2014 (Table 1). In addition to the quality control, which included correction for adjacent effects and land masking, performed by USGS on the Landsat 8 data, we applied the cloud mask generated by USGS and a realistic coastline vector mask. The density of kelp was parameterized as the normalized difference vegetation index (NDVI), which was derived from the images using Band 4 (0.64 to 0.67 nm) and Band 5 (0.85 to 0.88 nm). NDVI is a standard vegetation index which has been used as a measure of kelp canopy density. For example, Cavanaugh et al. (2011) extracted kelp density from Landsat images by using multiple endmember spectra mixture analysis with which pixels in each image were modeled as a 2-endmember linear mixture of kelp and water (see Cavanaugh et al. 2010, 2011 for details). Following Cavanaugh et al. (2011), we used a threshold NDVI value of 0.13; higher values are classified as kelp-dominated. More detailed information of derivation and processing kelp concentration from Landsat images used in our study area can be found in ASL Environmental Sciences (2014).

The SST data were derived from the TIRS Band 10 (10.60 to 11.19 nm). Before converting the radiative signal into SST, an atmospheric correction was applied to account for uncertainty in the Landsat TIRS band (Schneider & Mauser 1996, Ferrier et al. 1997, Fisher & Mustard 2004). Following Thomas et al. (2002), the Landsat SST data were calibrated against SST derived from Aqua MODIS. Due to the large difference in the spatial resolution of Landsat and MODIS, Landsat images were projected onto the MODIS grid for all 9 scenes using the Beam Software package from the European Space Agency (www.brockmann-consult.de/cms/web/beam/). As expected, the raw comparison of both datasets gave a positive correlation coefficient (R) of 0.68 (N = 65 418); noise arises from various sources such as different satellite overpass times, possible presence of cloud cover and cloud edge, and the projection of Landsat data onto the MODIS grid. We applied a method similar to that of Thomas et al. (2002) to the combined 9 images to remove possible outliers by iteratively running a model-2 type regression and removing points with an absolute residual greater than the mean residual plus 1 SD. The resulting number of points after an iterative procedure was reduced to 41 264. This procedure gave an R^2 of 0.98, a slope of 1.02, and an intercept of 2.66°C (Fig. 2). We applied these pseudo-calibration coefficients to Landsat imagery to retrieve SST.

Mixed-layer model

The satellite images of Landsat only provide the temperature at the sea surface, and the vertical distribution of temperature in the water column is not known. Therefore, we introduced a 1-D mixed layer model developed by Price et al. (1986), with which

Table 1. Summary statistics for individual images. Dates are given as yy-mm-dd. NDVI: normalized difference vegetation index, SST: sea surface temperature, Npts: number of pixel points

Image date	Day of year	NDVI > 0.13					NDVI < 0.13					ΔSST (°C)
		NDVI		SST (°C)		Npts	NDVI		SST (°C)		Npts	
		Avg	SD	Avg	SD		Avg	SD	Avg	SD		
2013-04-15	105	0.45	0.16	9.67	1.26	3195	−0.08	0.05	7.93	0.37	20851	1.74
2013-05-26	146	0.36	0.15	11.75	1.37	1839	−0.31	0.10	9.27	0.54	22204	2.48
2013-07-13	194	0.54	0.18	12.81	1.77	3904	−0.34	0.11	10.72	0.56	20100	2.09
2013-07-29	210	0.39	0.16	12.51	2.02	3798	−0.10	0.07	10.61	1.07	20248	1.90
2014-05-04	124	0.43	0.16	10.83	1.62	2984	−0.05	0.04	8.50	0.47	21032	2.33
2014-06-05	156	0.39	0.15	8.87	1.54	3244	−0.03	0.03	7.21	1.01	20738	1.65
2014-07-23	194	0.32	0.16	13.98	0.89	1086	−0.04	0.05	12.73	0.46	22961	1.25
2014-08-17	229	0.33	0.13	10.37	1.88	2458	−0.07	0.05	7.01	2.49	19001	3.36
2014-09-02	245	0.34	0.14	13.44	0.95	2971	−0.13	0.06	12.38	0.39	21046	1.06

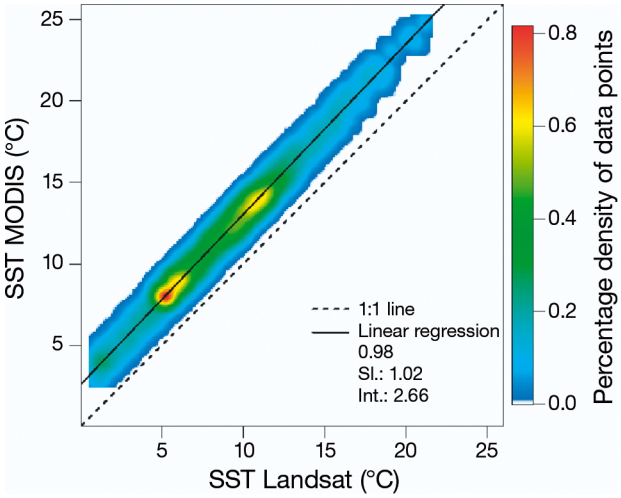

Fig. 2. Comparison of sea surface temperature (SST) derived from MODIS and from Landsat for all 9 images used in the study; sl.: slope, int.: intercept. Correlation coefficient R = 0.98

the vertical variation in temperature and solar radiation was investigated. The model was forced by winds and heat fluxes. In the model, SST is estimated in the upper mixed layer by the balance between buoyancy due to the density stratification and velocity shear caused by wind forcing. Following Price et al. (1986), the temperature, salinity, and momentum balance can be written as

$$\frac{\partial T}{\partial t} = -\frac{1}{\rho_0 c_p}\frac{\partial F_H}{\partial z} \quad (1a)$$

$$\frac{\partial S}{\partial t} = -\frac{\partial F_W}{\partial z} \quad (1b)$$

$$\frac{\partial \mathrm{v}}{\partial t} + f \times \mathbf{v} = -\frac{1}{\rho_0}\frac{\partial G}{\partial z} \quad (1c)$$

where T (°C), S, and $\mathbf{v}$ represent the temperature, salinity, and horizontal velocity vector; t (s) is time, ρ_0 (kg m^{-3}) and c_p (J [kg K]$^{-1}$) are the density and heat capacity of seawater, and f is the Coriolis parameter. The terms F_H (W m^{-2}), F_W, and G represent the fluxes of heat, freshwater (m), and momentum (m^2 s^{-2}). At the sea surface, F_H (0) = Q, which corresponds to the net heat flux; F_W (0) = $S(E - P)$, which corresponds to the surface salinity times the net freshwater flux (evaporation rate minus precipitation rate); and $G(0)$ = τ is the wind stress. In addition to the longwave radiation and sensible and latent heat fluxes, which represent the heat exchange due to reflection, convection, and evaporation, respectively, the net heat flux includes the downward shortwave solar radiation, whose depth distribution can be described as a sum of 2 exponential formulas (Paulson & Simpson 1977):

$$I(z) = \alpha I(0)e^{(-z/\lambda_1)} + (1-\alpha)I(0)e^{(-z/\lambda_2)} \quad (2)$$

Where $I(0)$ is the downward solar radiation at the sea surface. The first term on the right side represents the red spectral (non-penetrating) component, which in general attenuates within the top few centimeters. The second term represents the penetrating, blue-green spectral component, which attenuates at tens of meters depending on water turbidity. The variable α is the fraction of the non-penetrating component, and λ_1 and λ_2 are the extinction depths of the non-penetrating and penetrating components, respectively. Following Paulson & Simpson (1977), we used α = 0.62, λ_1 = 0.6 m and λ_2 = 20 m for clear water.

In order to include the effect of kelp on downward irradiance, the value of λ_2 in kelp areas is estimated based on the *in situ* data of Gerard (1984). The data consist of canopy density, defined as the blade area per bottom area (m^2 blade m^{-2}), and downward shortwave solar radiation (400–700 nm) at 1 m below the kelp canopy. Gerard (1984) measured the solar radiation at 1 m below kelp canopy with 2 quantum scalar profiling systems with spherical underwater sensors. The data were collected during June to August 1983 at 6 locations under sunny conditions within 2 *Macrocystis pyrifera* forests at Palos Verdes and Laguna Beach, California, USA. The canopy density was determined by the mean frond density × mean canopy length × mean blade area per canopy length. The recording time at each location varied from 80 to 225 min. To determine the relationship between solar radiation and kelp concentration, one can estimate the extinction depth by fitting solar radiation observations made throughout the water column, which is covered by the kelp canopy with specific concentrations. However, the solar radiation data collected by Gerard (1984) were at only 2 depths, at the sea surface and 1 m below the sea surface. Therefore, in this study, using the data of Gerard (1984), a relationship between NDVI and the extinction depth of λ_k due to kelp was derived based on 2 assumptions: (1) the canopy density is assumed to be proportional to the NDVI (Fig. 3A); and (2) the relation between the light fraction and the NDVI at 1 m depth can be written as an exponential form of

$$I(1) = I(0) \times e^{\left(-\frac{\mathrm{NDVI}-0.13}{k}-\frac{1}{\lambda_2}\right)} = I(0) \times e^{\left(\frac{-1}{\lambda_k}\right)} \quad (3)$$

and

$$\frac{1}{\lambda_k} = \frac{(\mathrm{NDVI}-0.13)}{k} + \frac{1}{\lambda_2} \quad (4)$$

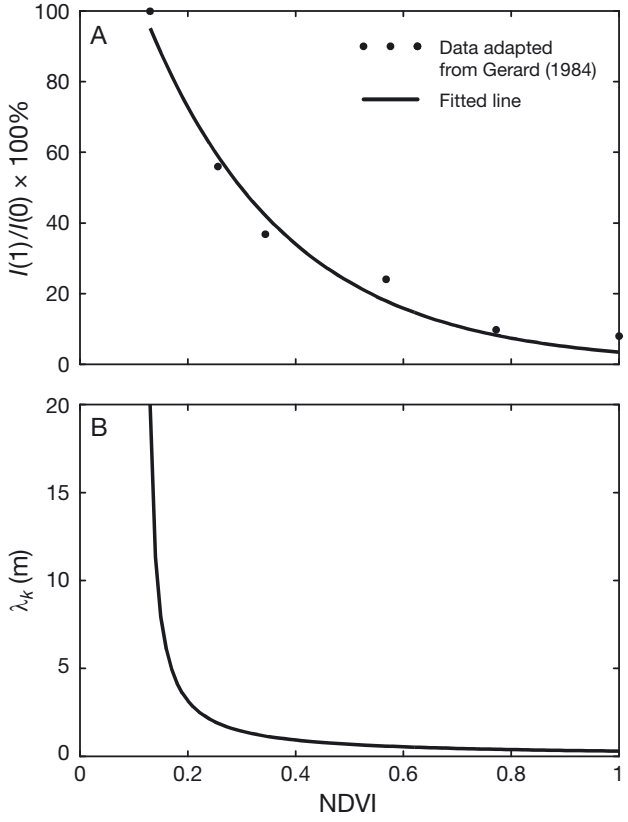

Fig. 3. (A) Fitted line of light fraction at 1 m and the normalized difference vegetation index (NDVI). (B) Relation between extinction depth λ_k and NDVI, where $\frac{1}{\lambda_k} = \frac{(\mathrm{NDVI} - 0.13)}{k} + \frac{1}{\lambda_2}$

where k = 0.263 m is a fitted constant, derived using a nonlinear least squares method. The fitted line based on the relation between λ_k and NDVI is plotted in Fig. 3B. The first term on the right hand side of Eq. (4) represents the attenuation of light due to kelp and the second term is the attenuation due to seawater. Since a threshold value of NDVI of 0.13 was used (Eq. 4), the relationship is only valid for NDVI values greater than 0.13.

The extinction depth changes rapidly from 20 m in kelp-free water to about 2 m in water with NDVI of 0.3, whereupon the extinction depth decreases more slowly in a quasi-linear fashion. Thus, we expected a rapid increase in SST for NDVI values in the range of about 0.13–0.30, with a slower increase for values of NDVI exceeding 0.30. Using the extinction depth λ_k, the distribution of the penetrative component of solar radiation with water depth can be calculated. For cases where the penetration depth due to kelp is less than the penetration depth of the non-penetrating radiation, i.e. $\lambda_k < \lambda_1$, we set $\lambda_1 = \lambda_k$.

The mixed layer model was initialized with climatological temperatures and salinities from a seasonal data set covering the Northeast Pacific Ocean based on the analysis of Foreman et al. (2008). The climatological dataset has 52 vertical layers, 5 within the upper 30 m. There are 3 grid points (Fig. 1) in our study area, Sites 1 and 2, corresponding to a kelp bed, and Site 3 in open water; their vertical distributions of temperature and salinity of the mean winter and spring seasons are shown in Fig. 4. At all 3 sites, the temperature differences in winter and spring were within 0.02°C over the entire profile; on the other hand, salinity at Site 1, the most offshore location, was higher than at Sites 2 and 3 by <0.1. The mean temperature and salinity of these 3 grid points were used to initialize the model. Atmospheric forcing, including wind speed, air temperature, relative humidity, precipitation rate, and solar radiation at the sea surface used in the model were from the hourly output of a regional model with a spatial resolution of 2.5 km (Mailhot et al. 2014). Wind stress was computed using the wind velocity and a neutral drag coefficient of Smith (1980); heat fluxes were computed using the bulk formula. The water depth of the model run was 30 m, and the vertical grid interval was 1 m.

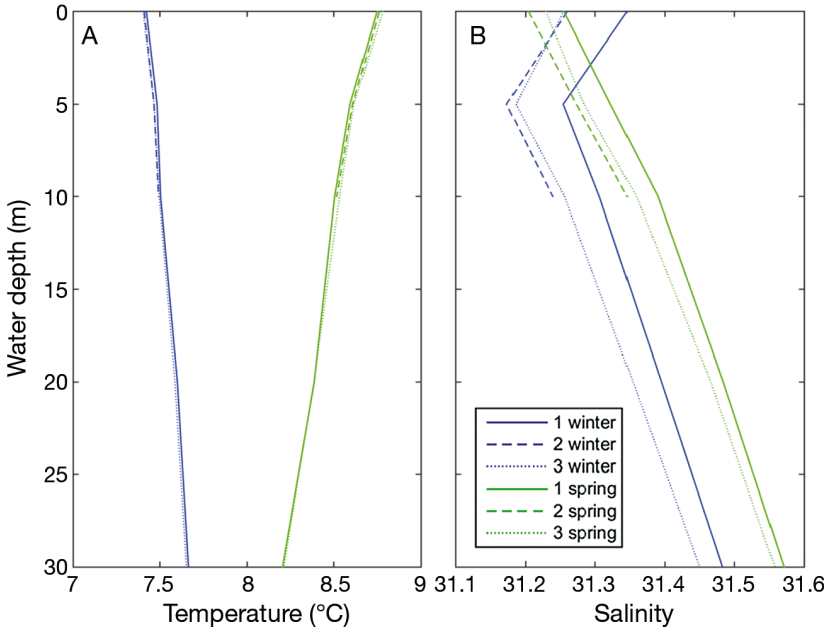

Fig. 4. (A) Temperature and (B) salinity at 3 locations (Sites 1, 2, and 3 in Fig. 1) in winter (blue) and spring (green) from Foreman et al. (2008)

The model was integrated from 1 April to 31 October 2013, with a time step of 15 min. Fourteen model runs were made with different NDVI values (0.0, 0.14, 0.15, 0.16, 0.18, 0.20, 0.25, 0.30, 0.40, 0.50, 0.70, 0.80, 0.90, and 1.00). The output was truncated to hourly intervals for subsequent analysis. We did not run the model for 2014 because atmospheric data were not available.

RESULTS

Observations

Two sample images of NDVI and SST from the spring and summer of 2013 are shown in Fig. 5. In spring, the region was dominated by low NDVI values with high values (or kelp) concentrated close to shore around islands (Fig. 5A). SST shows a similar spatial distribution, with lower temperatures in the open water and higher temperatures in the near-shore zone, especially in areas occupied by kelp (Fig. 5C). During summer, areas with NDVI >0.13 were more extensive and with larger amplitudes than those during spring (Fig. 5B); the spatial SST mirrors that of the NDVI distribution (Fig. 5D). In both seasons, SST differences between coastal and open ocean areas can be as much as ~6°C. The comparisons of SST and NDVI for the 2 images indicate that the SST in kelp areas (NDVI > 0.13) was higher than that in the ambient kelp-free waters (NDVI < 0.13). Despite considerable variability, the data show a trend of SST increasing with NDVI (Fig. 5E,F).

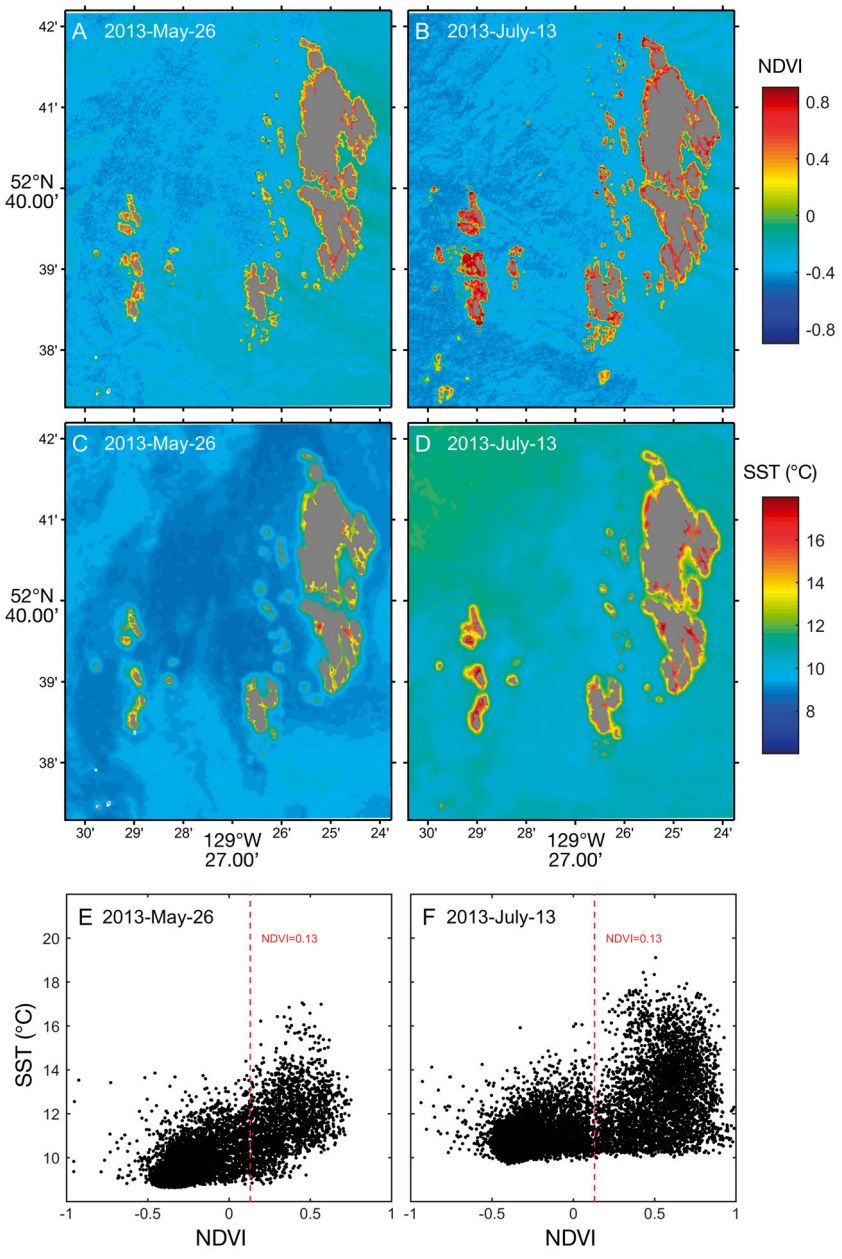

Fig. 5. Examples of (A,B) normalized difference vegetation index (NDVI) and (C,D) sea surface temperature (SST) in spring (A,C) and summer (B,D). (E,F) SST and NDVI for the depth range 5–30 m

The averages and standard deviations (SD) of SST and NDVI in both kelp (NDVI ≥ 0.13) and kelp-free (NDVI < 0.13) waters within depths of 5–30 m for the individual images are given in Table 1. For kelp areas, mean NDVI values vary from 0.32 to 0.54 with SDs of 0.13 to 0.18. Mean SSTs in kelp areas vary from 8.9 to 14.0°C and corresponding SDs from 0.9 to 2.0°C. In the non-kelp areas, mean NDVI values are negative from all images, varying from –0.34 to –0.03 with SD from 0.03 to 0.11. The mean SSTs vary from 7.0 to 12.7°C with SD of 0.4 to 2.5°C. All images show that the mean SST in the kelp areas is higher than in the non-kelp areas. The mean magnitude of the increase for the 9 images is about 2.0°C and the maximum reaches 3.4°C.

The 9 images used in this study are from early spring to late summer over a 2 yr period when mean SST can differ by ~7°C in the study region and the SD by a factor of ~6 (Table 1). To compare and potentially combine datasets, we normalized SST using the *Z*-transform (ztf):

$$SST_{ztf}^{i,j} = \frac{SST^{j}(i) - SST_{avg}^{j}}{SD^{j}} \quad (5)$$

where i and j indicate the i^{th} pixel in the j^{th} image, respectively. The subscript *avg* represents the average SST in image *j*. The transformed images have mean normalized SSTs of 0 and SDs of 1. After transformation, the images could be combined to determine if a systematic pattern emerges. The transformed data for NDVI > 0.13 for the 9 images are shown in Fig. 6. For all images, SST_{ztf} increases with increasing NDVI over most of the range; some images show a decrease in SST_{ztf} at high values of NDVI (>0.7 or 0.8). There is considerable scatter in all of the images. While the overall tendency in all of the images is for SST to increase almost linearly with increasing NDVI, particularly for NDVI < 0.6, the fitted lines account for only 10 to 28% of variances in SST. There are 4 images where more than 20% variances are accounted for (Fig. 6D,F,H,I). The increases in SST are reduced for NDVI > 0.60 and even decrease (NDVI > 0.8) for some images, particularly for 13 July 2013, when NDVI accounts for the least amount of variance of all the images (Fig. 6C).

The increased SST due to the presence of kelp can be estimated by comparing the SST of the endpoint of the fitted line (see Table 2 for filter characteristics) and the SST in the non-kelp area. The results indicate that SST in kelp areas is higher than that in non-kelp areas (Table 2). The kelp enhances the SST by 0.2 to 5.4°C, with a mean (median) value of 2.7°C (2.9°C) and SD of 1.4°C. The fitted curves with 1 exception generally increase from lower to higher NDVI values, with some leveling off at the high end of the curve. This implies that changes in SST are also controlled by mechanisms other than the heat absorption effect of kelp. In Fig. 6, there is a strip with approximately constant normalized SST at the bottom of some images (e.g. Fig. 6C,I). This may be

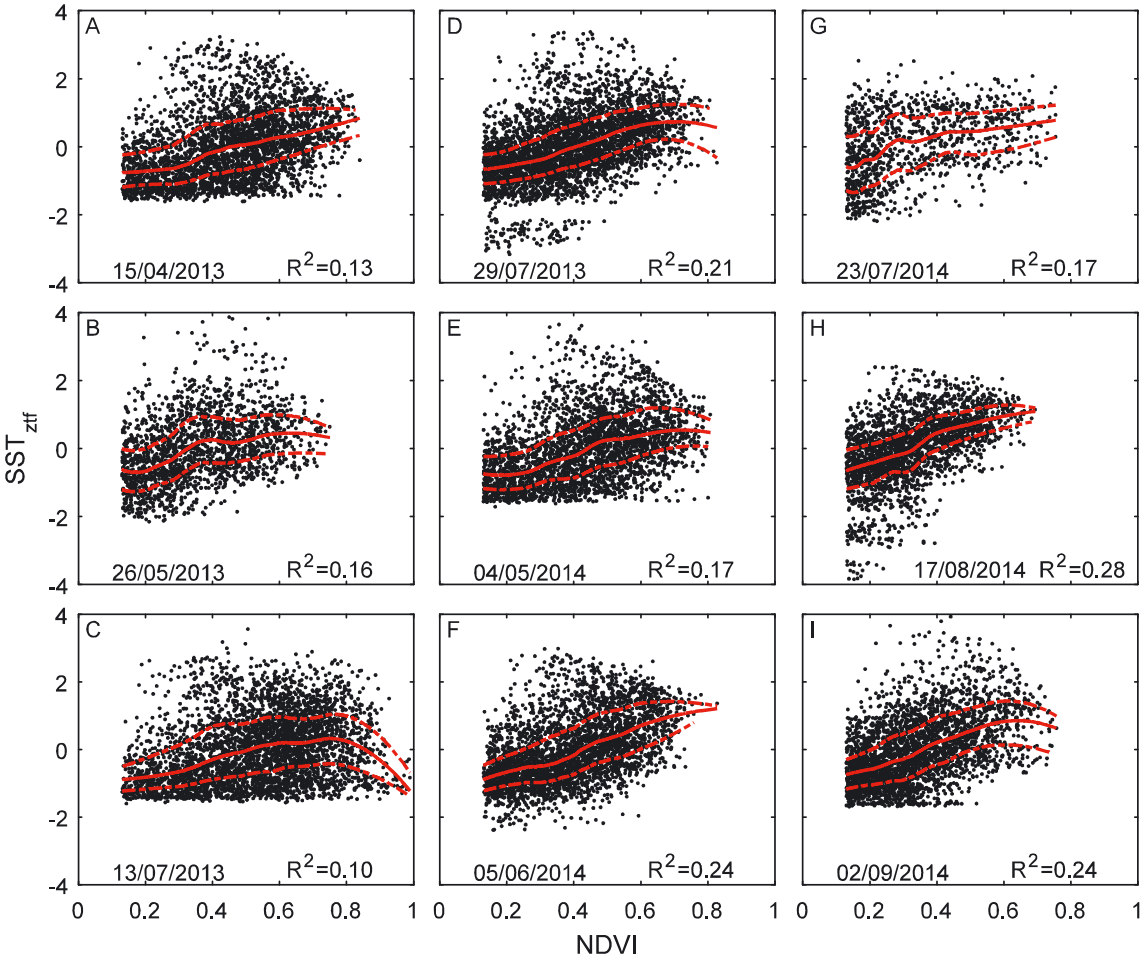

Fig. 6. *Z*-transformed sea surface temperature (SST_{ztf}) and normalized difference vegetation index (NDVI > 0.13) from Landsat images. Solid red lines are from a linear Loess (40%) filter. Dash-dot lines represent a moving window estimate of the standard deviations. Dates are given as dd/mm/yy

Table 2. Comparison of sea surface temperature (SST) from the normalized difference vegetation index (NDVI < 0.13) and endpoint SST from a Loess filter (linear, 40%). Dates are given as yy-mm-dd

Image date	SST from NDVI < 0.13 (°C)	SST from Loess (°C)		SST difference (°C)
		NDVI at Loess endpoint	SST at Loess endpoint (°C)	
2013-04-15	7.93	0.84	10.74	2.81
2013-05-26	9.27	0.75	12.20	2.93
2013-07-13	10.72	0.99	10.87	0.15
2013-07-29	10.61	0.83	13.65	3.04
2014-05-04	8.50	0.81	11.59	3.09
2014-06-05	7.21	0.83	10.73	3.52
2014-07-23	12.73	0.75	14.68	1.95
2014-08-17	7.01	0.69	12.43	5.42
2014-09-02	12.38	0.76	14.03	1.65

explained by the horizontal advection and enhanced mixing rather than solely by local solar heating. The SSTs of points in this region are close to the background SST, which is defined as the mean SST at a water depth >30 m (Fig. 7A,B). Moreover, there is some consistency in their locations from one image to another. The pixels with SST lower than the background value are mainly distributed around small isolated islands.

The fits of SST as a function of NDVI for the 9 images are summarized in Fig. 8. It is apparent that transforming

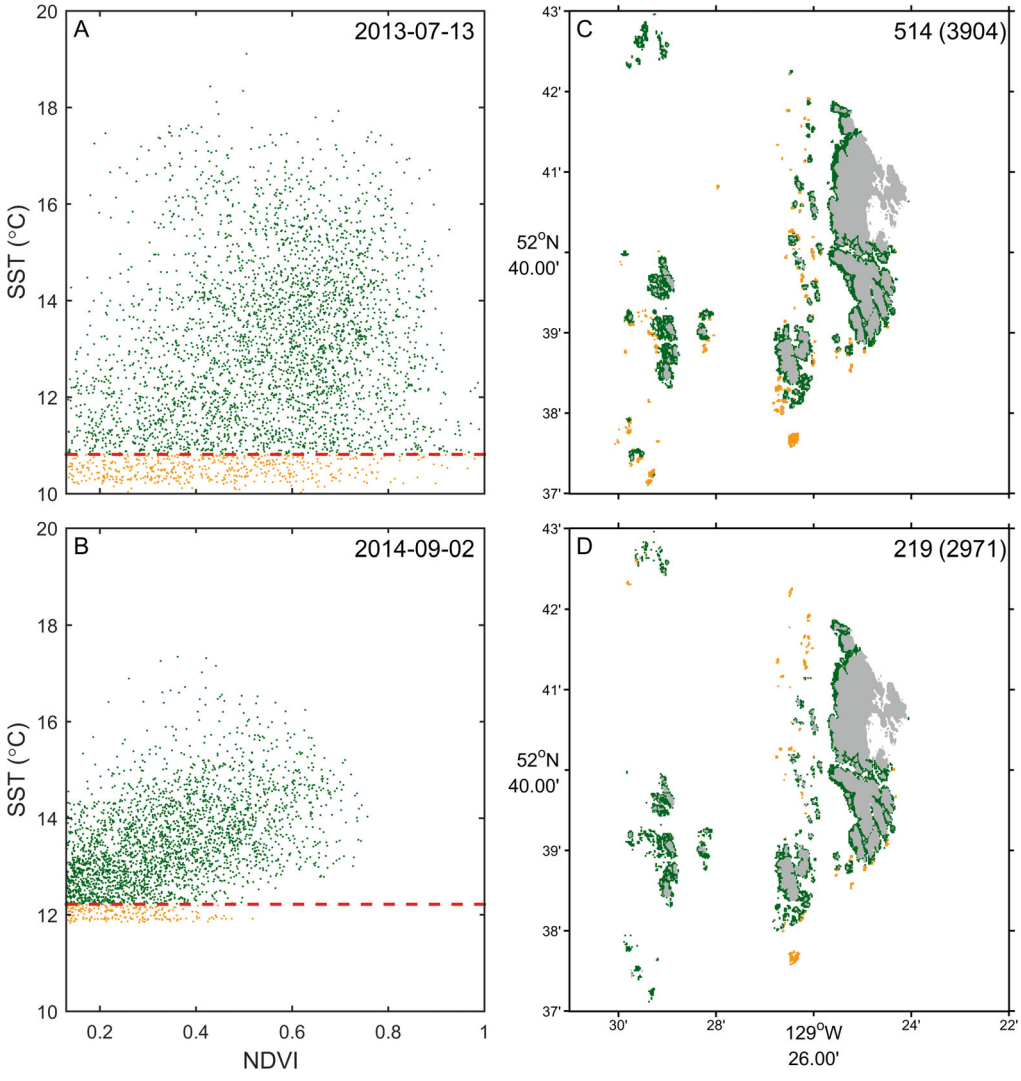

Fig. 7. (A,B) Sea surface temperature (SST, orange dots) lower than open-ocean SST and (C,D) their spatial distributions on 13 July 2013 (A,C) and 2 September 2014 (B,D). Dashed red lines in A and B indicate offshore SST defined as the mean SST of water with depths >30 m in our study domain (see Fig. 1). Numbers (upper right corners in C,D) are the number of orange points and (in parentheses) the total number of points

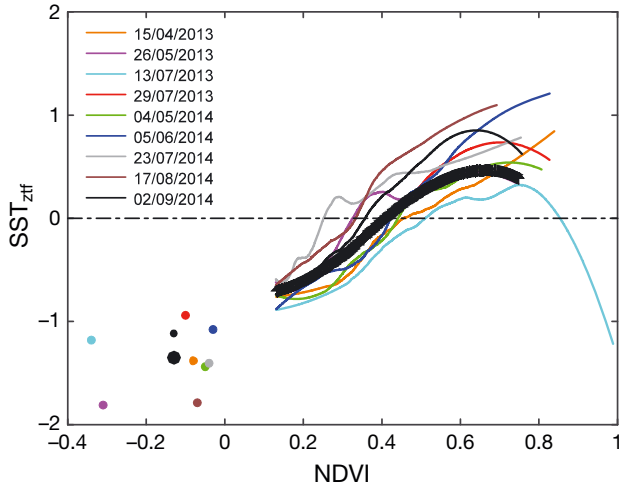

Fig. 8. Loess filter lines of individual LANDSAT images. The thick black line is the composite of the 9 fits. Dots are the mean *Z*-transformed sea surface temperature (SST_{ztf}) for all points where the normalized difference vegetation index (NDVI) < 0.13. The large black dot is the composite mean. Dates are given as dd/mm/yy

the SST data for the 9 images, where the ranges for the areas where NDVI > 0.13 (< 0.13) of average SST is 5.1°C (5.7°C) and the ratio of SDs is 2.3 (6.7, see Table 1), is successful in collapsing the result into a compact representation. The composite curve shows a nearly linear relationship between SST and NDVI for NDVI ranging between 0.13 and 0.60. Two images (13 July 2013 and 02 September 2014) are the main contributors to the levelling off and downturn of the composite curve. This decrease in SST indicates that SST in kelp areas is also controlled by other mechanisms, for example vertical mixing, which we will discuss next.

Since kelp grows mainly in shallow water, one could argue that the depth could be the main reason for the higher SST. To address this argument, we plotted SST_{ztf} versus water depth in Fig. 9. For the 9 images, the R^2 between SST_{ztf} and water depth ranges from 0.01 to 0.04, indicating an extremely weak relationship between SST and bottom depth.

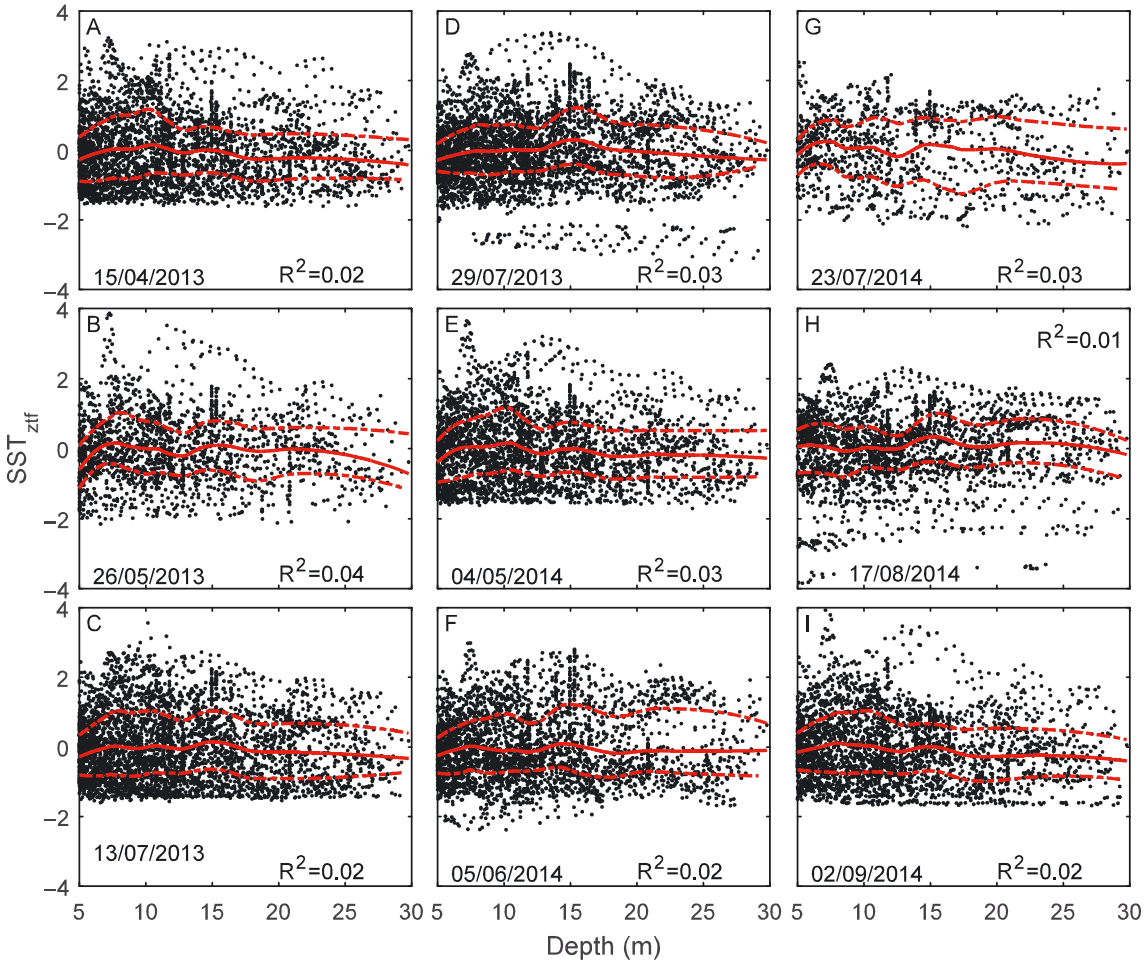

Fig. 9. *Z*-transformed sea surface temperature (SST_{ztf}) and depth for the range of 5–30 m. Solid red lines are from a linear Loess (40%) filter. Dash-dot lines represent a moving window estimate of the standard deviations. Dates are given as dd/mm/yy

Model

Comparison with observations

A direct comparison of SST between the model and Landsat images is not possible because spatial variations in the initial conditions of temperature and salinity and the atmospheric forcing in the kelp forests are not available. We therefore used an indirect approach. Using the model and the satellite data of SST and NDVI, comparisons of SST_{ztf} (Eq. 5) between model results and the 4 images collected in 2013 are plotted in Fig. 10. The modeled *Z*-transformed SSTs are derived from the daily mean SSTs of the 14 model runs with NDVI varying from 0 to 1.0. Modeled relationships between SST and NDVI in general capture the tendency of SST to increase with increasing NDVI. Both the model and observations show that SST increases more rapidly for low values of NDVI and tends to level off at higher values. The observations show considerable scatter throughout the entire range of NDVI values, perhaps attributable to spatial variations in the ocean temperature, salinity, and currents, and of atmospheric forcing not accounted for by the 1-D model. The correlation coefficients between the model results and observations range from 0.32 to 0.46, all higher than their 95% significant levels, but only capturing 10 to 21% of the variances.

The composite fit of the LANDSAT data and the model results are compared in Fig. 11. The model result increases rapidly from NDVI = 0.13 to ~0.3, then plateaus with little variation over the rest of the range, unlike the observations, which increase nearly linearly from NDVI = 0.13 to ~0.6 The root mean square difference between the model and observations is 0.46 (SD units) for NDVI ≥ 0.13; it is generally within the area defined by ±1 SD of the observations, except for NDVI values of 0.25–0.32, where the modeled SST_{zft} is slightly higher than the observations. The higher modeled SST_{zft} and its rapid increase over the lower range of NDVI is likely due to the shallow extinction depth used in the model (Fig. 4B).

NDVI and temperature: model simulations

Despite only qualitative agreement between the model predictions and the observations, further exploration of the model might provide some insight into how kelp could modify ocean temperature. The time series of SST from the model shows clear seasonal and high frequency variation from spring to summer, and their dependence on kelp concentrations (Fig. 12A). Compared to the non-kelp case, SST is in general higher and increases in magnitude for higher values of NDVI (Table 1), and these observed differences are also plotted in Fig. 12B. The modeled differences in SST due to kelp agree well with the observed counterparts except in early spring (15 April 2013), where high modeled values are likely due to an overestimation of the kelp effect in the model but also could be due to the initialization of the model using climatological conditions rather than the realized conditions in 2013. Perry (2014) indicated that SST at weather buoy C46185 (about 36 km SW of the islands) at the end of March 2013 was about 1°C below normal. This would bring the initial model–observation comparison into better agreement (Fig. 12). The differences between kelp-free modeled SST and 3 densities of kelp during spring and summer

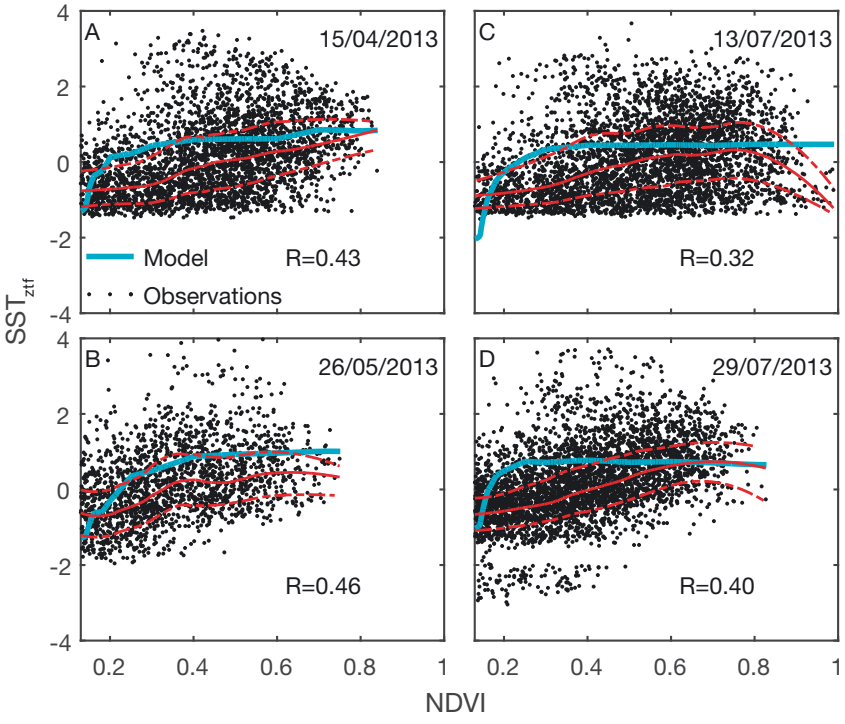

Fig. 10. Comparisons of observed (black dots) and modeled *Z*-transformed sea surface temperature (SST_{ztf}; blue line). Solid red lines are from a linear Loess (40%) filter. Red dash-dot lines represent a moving window estimate of the standard deviations. NDVI: normalized difference vegetation index. Dates are given as dd/mm/yy

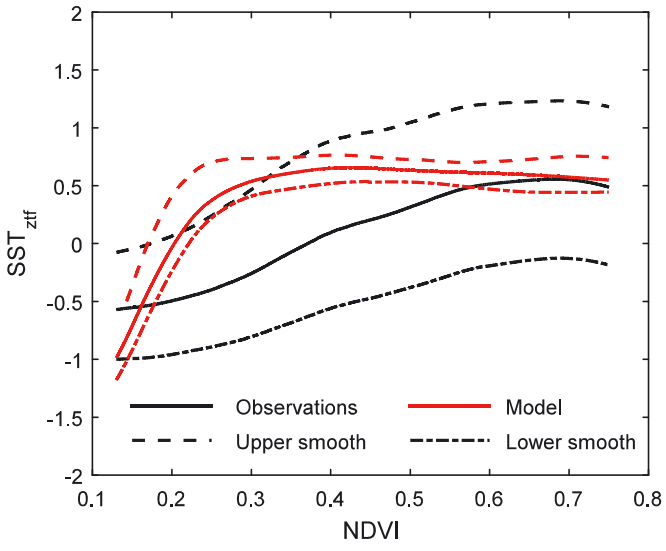

Fig. 11. Comparison of composite *Z*-transformed sea surface temperature (SST_{ztf}) with Loess filter from observations (black) and model results (red). NDVI: normalized difference vegetation index

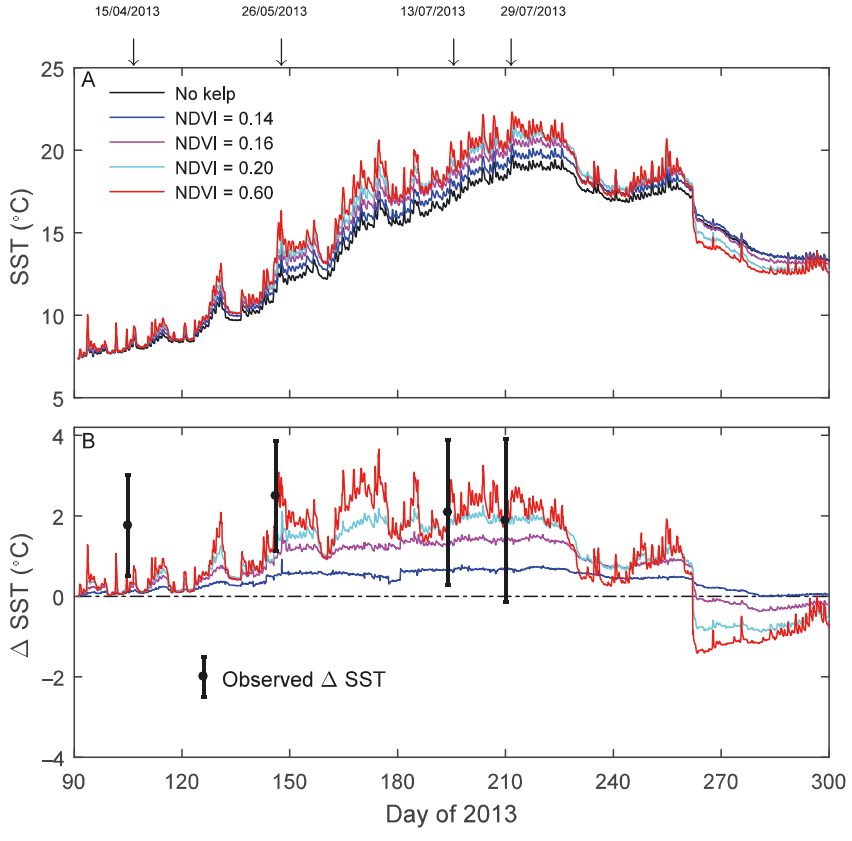

Fig. 12. (A) Sea surface temperature (SST) and (B) SST difference between model runs with and without kelp. The black bars in B indicate the observed SST differences (dot) ± 1 SD given in Table 1. NDVI: normalized difference vegetation index

showed some surprising results (Table 3). In spring (day of year [DOY] 90–180), the mean SSTs are 1.11, 1.12, and 1.14°C higher for NDVI = 0.20, 0.60, and 0.90, with SDs of 0.88, 0.90, and 0.92°C, respectively. The maximum differences are 3.45, 3.66, and 3.82, and the minima are 0. This means that in spring the SST when kelp is present is always higher than that in the kelp-free case. In summer (DOY 180–270), the mean differences are about 1.31°C and SDs are from 1.02 to 1.08°C. The maximum differences are 3.01, 3.20, and 3.32°C and, in contrast to the spring results, the minima in summer are −1.38, −1.41, and −1.43°C. The negative differences are interesting since they indicate that SSTs in the kelp cases can be lower than those in the kelp-free area, which shows that processes other than surface heating must play a role in determining the SST.

Time series of temperature profiles from the model for cases with and without kelp are plotted in Fig. 13. Temperature in the upper mixed layer shows seasonal variation, increasing from spring to summer and then decreasing for all cases with and without kelp. In early spring (DOY 90–120), temperature is low and the mixed layer depth (MLD) is up to 30 m. The MLD is defined here as a temperature difference of 0.2°C between the surface and that at the base of the mixed layer. With the increase in solar radiation from spring to summer, water with a kelp canopy stratifies earlier and shallower, and the temperature in the mixed layer is higher than that in the kelp-free case. Temperatures are higher with higher NDVI. The MLDs in kelp cases are shallower compared to the kelp-free case, especially in the middle of summer, where it is about 8 m in the case of NDVI = 0.6, about 50% shallower than the case with no kelp. The shallow MLD is due to more heat absorbed in the surface layer by kelp. By the end of summer, however, the MLD suddenly deepens, and SST drops for all the model runs. The SST for NDVI = 0.6 is lower than that in the kelp-free case by about 2°C.

Mixing and temperature

At the end of summer, the MLD increased and SST dropped due to a

Table 3. Comparison of the change in sea surface temperature (ΔSST) between model runs with and without kelp present in spring and summer. NDVI: normalized difference vegetation index

NDVI	Spring (ΔSST, °C)				Summer (ΔSST, °C)			
	Mean	SD	Max	Min	Mean	SD	Max	Min
0.2	1.11	0.88	3.45	0.0	1.31	1.02	3.01	−1.38
0.6	1.12	0.90	3.66	0.0	1.30	1.06	3.26	−1.41
0.9	1.14	0.92	3.82	0.0	1.31	1.08	3.32	−1.43

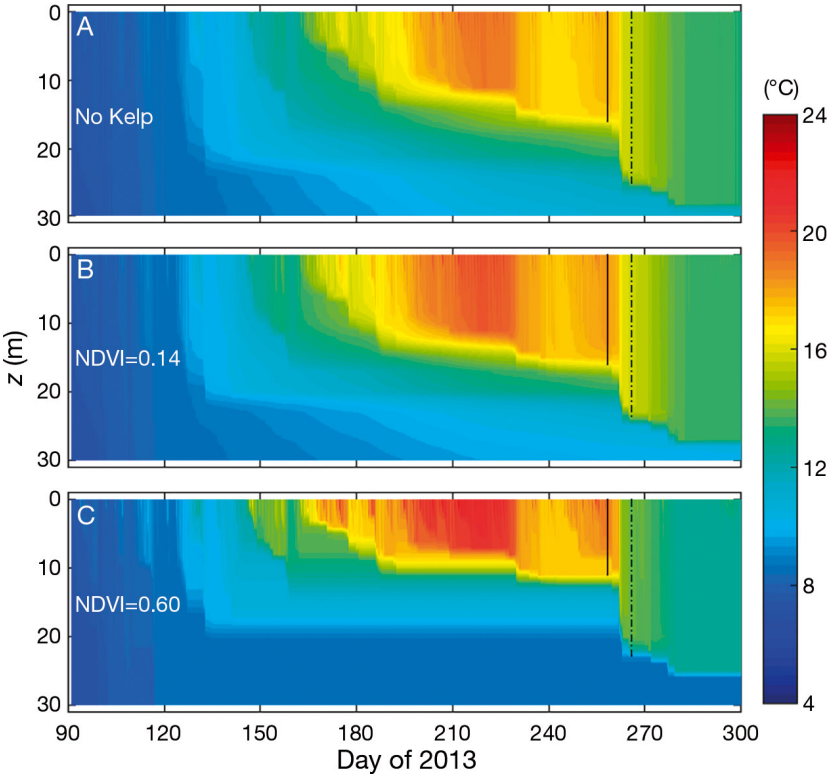

Fig. 13. Temperature distributions of cases of (A) no kelp, (B) normalized difference vegetation index (NDVI) = 0.14, and (C) NDVI = 0.60. The vertical solid and dashed lines indicate the mixed layer depth before and after a strong wind occurred, respectively

Table 4. Mixed layer depth (Z_{MLD}) and temperature before and after a storm occurred around day of year 260 (see Figs. 12 & 13). Subscripts 1 and 2 indicate the variables before and after the storm, respectively. NDVI: normalized difference vegetation index, SST: sea surface temperature, *T*sub: mean temperature in the layer between Z_1 and Z_2 before the storm

NDVI	Z_{MLD} (m)		Mean temp. (°C)		$Term_1$	$Term_2$	Total	SST_2
	Z_1	Z_2	SST_1	T_{sub}	(°C × m)	(°C × m)	(°C × m)	(°C)
No kelp	16	25	17.6	14.1	282	127	409	16.4
0.14	16	24	18.1	13.9	290	111	401	16.7
0.60	11	23	18.4	10.9	202	137	333	14.5

storm on DOY 260 (Fig. 13A). According to Wu et al. (2007), temperature from the model in the upper mixed layer after a storm can be estimated by:

$$SST_2 = \frac{1}{Z_2}(Z_1 \times SST_1) + \frac{1}{Z_2}(Z_2 - Z_1) \times T_{sub} \quad (6)$$

where SST_1 and SST_2 are the mean temperatures in the mixed layer before and after storms; Z_1 and Z_2 are the MLDs before and after the storm, respectively. T_{sub} is the mean temperature in the layer between Z_1 and Z_2 before the storm. The first term on the right hand side is the contribution from water in the mixed layer before a storm, and the second term is the contribution of the MLD deepening. The magnitudes of the variables in Eq. (7) are listed in Table 4. Before the storm, MLD for the kelp-free case is about 16 m, close to that of the kelp case of NDVI = 0.14, but about 45% deeper than that in the case of NDVI = 0.60 of 11 m. After the storm, the MLD in the kelp-free cases is 25 m, 1–2 m deeper than those of kelp cases. Before the storm, SST is 17.6 °C in the kelp-free case, slightly lower than the kelp cases of 18.1 and 18.4°C. In the kelp-free case, T_{sub} is about 14°C, slightly higher than that for NDVI = 0.14, but considerably higher than 10.9°C, the temperature at NDVI = 0.60. The low temperature in the sub-surface layer is the consequence of the shading effect of kelp, which absorbs more solar radiation at the surface than in the case of clear water. The contribution of the mixed layer (Z_1 × SST_1) to the post-storm conditions, defined as $Term_1$ in Table 4, in the clear water case is 282°C × m, slightly lower than that of NDVI = 0.14, but 40% higher than that of NDVI = 0.60. The low value of $Term_1$ for NDVI = 0.6 is attributed to the shallower MLD despite slightly higher SST. The shallowing of the MLD and the increasing of SST are not symmetric. The presence of kelp results in a shallower MLD by 45%, but

only increases SST by 5%. The value of $Term_1$ in the case of NDVI = 0.14 is 290°C × m, higher than other cases because of the higher SST and the comparable MLD to kelp-free case. The value of ($[Z_2 - Z_1] \times T_{sub}$), $Term_2$ in Table 4, is 127°C × m in the kelp-free case, higher than for NDVI = 0.14, but lower than for NDVI = 0.60. The higher $Term_2$ for NDVI = 0.60 is clearly due to the greater increase (12 m versus 9 and 8 m for no kelp and NDVI = 0.14) of the MLD despite the lower temperature of 10.9°C. We conclude that variation in SST in waters with kelp is not only related to the increased SST due to surface trapping of heat, but is also related to the temperature below the mixed layer and the deepening of the mixed layer driven by atmospheric forcing.

Effects of heat fluxes on SST

In the upper mixed layer, changes in SST are controlled by 2 related processes: (1) the penetrating solar irradiance and (2) the heat exchange between ocean and atmosphere at the sea surface. Here we discuss the modifications of heat flux due to the presence of kelp. The time series of wind stress and heat flux (positive corresponds to heat transfer from ocean to atmosphere), defined as the sum of longwave radiation, latent heat, and sensible heat, clearly shows a strong wind event at the end of summer (around DOY 260) when the magnitude of wind stress reaches 0.8 Pa (Fig. 14A). The heat flux shows seasonal variation both for the cases with and without kelp (Fig. 14B). In the kelp-free case, the mean heat flux is 98 W m^{-2} in spring and 157 W m^{-2} in summer. The mean flux in spring (summer) is 107 (175) for NDVI of 0.14, and 128 (196) W m^{-2} for NDVI of 0.60. This means that the presence of kelp leads to more heat transfer from the ocean to the atmosphere, 30 W m^{-2} more in spring, and 39 W m^{-2} more in summer for NDVI = 0.6, about 31 and 25% greater than that of the kelp-free case. The integrated difference of heat flux in the model runs (kelp − kelp-free) reaches 1.8 × 10^8 J m^{-2} for NDVI = 0.14 and 5.3 × 10^8 J m^{-2} for NDVI = 0.60 by the end of summer (Fig. 15). The increased heat flux from the ocean to the atmosphere will raise the local air temperature; further investigation of the air temperature due to kelp heating, however, is beyond the scope of this study.

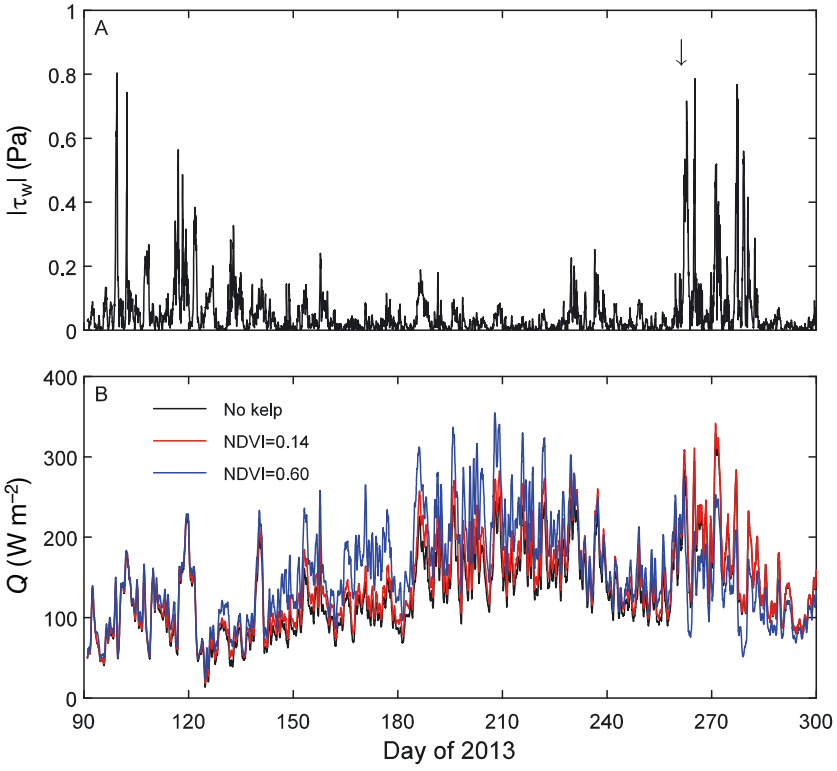

Fig. 14. (A) Time-dependent wind stress and (B) heat flux (sum of longwave radiation and sensible and latent heat flux; positive values indicate heat transfer from ocean to air). The black arrow in A denotes a storm. NDVI: normalized difference vegetation index

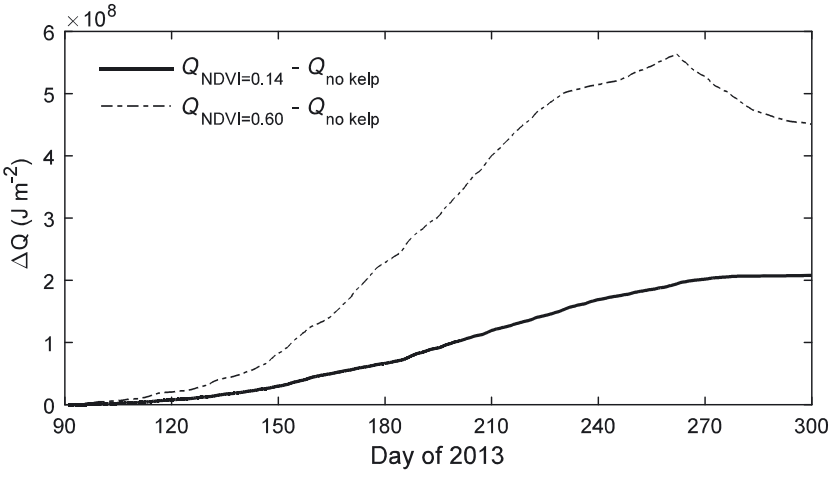

Fig. 15. Integrated model heat flux (longwave + sensible + latent) differences due to kelp. NDVI: normalized difference vegetation index

SUMMARY

SST in kelp forests was examined using observational data and a 1-D mixed layer model. The observations consistently indicate that SST increases with increasing NDVI with a maximum asymptotic value of 5.4°C and a median of 2.7°C (SD = 1.4°C). The relationship between SST and NDVI is nearly linear; however, it only accounts for 10–28 % of the variance, indicating considerable scatter. Model results indicate that the presence of kelp confines the absorption of solar shortwave radiation in the upper layer, increasing SST, resulting in a shallower MLD and enhancing the heat flux from ocean to atmosphere. At the same time, the model demonstrated that the SST with kelp present is strongly related to vertical mixing events; the change in SST in such situations is controlled not only by extra heat trapped by kelp, but also by the temperature in the sub-mixed layer and the deepening of the mixed layer.

In the model, the extinction depth due to kelp was based on several assumptions: (1) a linear relationship exists between the NDVI and frond density; (2) the extinction parameter is independent of water depth; and (3) the horizontal variation of processes, such as advection and diffusion, plays a minor role in determining SST in kelp forests. Moreover, the relationship between light attenuation due to kelp and NDVI is based on few, non-contemporaneous *in situ* observations. The scatter of SST observations with increasing NDVI values, and in particular the low values of SST anomalies over a broad range of increasing NDVI, indicates that these assumptions, particularly the lack of spatial dependence, need further examination beyond a 1-D model. Nonetheless, the current model has captured some of the physics governing SST variability in the presence of kelp.

While the model in this preliminary study captured some of the dynamics, the scatter of the SST observations for all NDVI values remains problematic. More *in situ* data on kelp concentrations, ocean currents, and mixing strengths, and contemporaneous observations of NDVI would be valuable to determine if the scatter of SST about the empirical fit and model predictions could be reduced. Given the variability in the SST response throughout the entire range of NDVI values, it appears that this would require a major field and modeling effort.

Acknowledgements. This research was supported by the World Class Tank Safety System Program of the Federal Government of Canada. We thank C. Caverhill and V. Stuart for comments on the draft manuscript. We also thank P. Thupaki for providing atmospheric data.

LITERATURE CITED

Arkema KK, Reed DC, Schroeter SC (2009) Direct and indirect effects of giant kelp determine benthic community structure and dynamics. Ecology 90:3126–3137

ASL Environmental Sciences (2014) Compilation and processing of LANDSAT image data for mapping eastern Hecate Strait, British Columbia. Phase 1, PR-840. ASL Environmental, Saanichton, BC

Cavanaugh KC, Siegel DA, Kinlan BP, Reed DC (2010) Scaling giant kelp field measurements to regional scales using satellite observations. Mar Ecol Prog Ser 403: 13–27

Cavanaugh KC, Siegel DA, Reed DC, Dennison PE (2011) Environmental controls of giant-kelp biomass in the Santa Barbara Channel, California. Mar Ecol Prog Ser 429:1–17

Chen J, Zhu Y, Wu Y, Cui T, Ishizaka J, Ju Y (2015) A neural network model for $K(\lambda)$ retrieval and application to global K_{par} monitoring. PLOS ONE 10:e0127514

Dayton PK (1985) Ecology of kelp communities. Annu Rev Ecol Syst 16:215–224

Druehl LD (1978) The distribution of *Macrocystis integrifolia* in British Columbia as related to environmental parameters. Can J Bot 56:69–79

Ferrier AF, Lee M, Anderson WB, Benvenuto G, Morrison DK, Lowy DR, DeClue JE (1997) Sequential modification of serines 621 and 624 in the Raf-1 carboxyl terminus produces alterations in its electrophoretic mobility. J Biol Chem 272:2136–2142

Fisher JI, Mustard JF (2004) High spatial resolution sea surface climatology from Landsat thermal infrared data. Remote Sens Environ 90:293–307

Foreman MGG, Crawford WR, Cherniawsky JY, Galbraith J (2008) Dynamic ocean topography for the northeast Pacific and its continental margins. Geophys Res Lett 35: L22606

Fram JP, Stewart HL, Brzezinski MA, Gaylord B, Reed DC, Williams S, MacIntyre S (2008) Physical pathways and utilization of nitrate supply to the giant kelp, *Macrocystis pyrifera*. Limnol Oceanogr 53:1589–1603

Gaylord B, Reed DC, Raimondi PT, Washburn L, McLean SR (2002) A physically based model of macroalgal spore dispersal in the wave and current-dominated nearshore. Ecology 83:1239–1251

Gaylord B, Rosman JH, Reed DC, Koseff JR, Fram JP, MacIntyre S, Monismith SG (2007) Spatial patterns of flow and their modification within and around a giant kelp forest. Limnol Oceanogr 52:1838–1852

Gaylord B, Nickols KJ, Jurgens L (2012) Roles of transport and mixing processes in kelp forest ecology. J Exp Biol 215:997–1007

Gerard VA (1984) The light environment in a giant kelp forest: influence of *Macrocystis pyrifera* on spatial and temporal variability. Mar Biol 84:189–195

Gruber RK, Kemp M (2010) Feedback effects in a coastal canopy-forming submersed plant bed. Limnol Oceanogr 55:2285–2298

Jackson GA (1987) Modelling the growth and harvest yield of the giant kelp *Macrocystis pyrifera*. Mar Biol 95:611–624

Jackson GA, Winant CD (1983) Effect of a kelp forest on coastal currents. Cont Shelf Res 2:75–80

Lobban CS (1978) Growth of *Macrocystis integrifolia* in Barkley Sound, Vancouver Island, BC. Can J Bot 56: 2707–2711

Mailhot J, Milbrandt JA, McTaggart-Cowan R, Erfani A, Denis B, Glazer A, Vallée M (2014) An experimental high-resolution forecast system during the Vancouver 2010 Winter Olympic and Paralympic Games. Pure Appl Geophys 171:209–229

Mann KH (1973) Seaweeds: their productivity and strategy for growth. Science 182:975–981

Nakamoto S, Kumar SP, Oberhuber JM, Muneyama K, Frouin R (2000) Chlorophyll modulation of sea surface temperature in the Arabian Sea in a mixed-layer isopycnal general circulation model. Geophys Res Lett 27:747–750

Paulson CA, Simpson JJ (1977) Irradiance measurements in the upper ocean. J Phys Oceanogr 25:474–495

Perry RI (ed) (2014) State of the physical, biological and selected fishery resources of Pacific Canadian marine ecosystems in 2013. Can Tech Rep Fish Aquat Sci 3102: 1–136

Pinsky ML, Greg G, Katie KA (2013) Quantifying wave attenuation to inform coastal habitat conservation. Ecosphere 4:95

Price JF, Weller RA, Pinkel R (1986) Diurnal cycling: observations and models of the upper ocean response to diurnal heating, cooling and wind mixing. J Geophys Res 91: 8411–8427

Reed DC, Foster MS (1984) The effects of canopy shading on algal recruitment and growth in a giant kelp forest. Ecology 65:937–948

Rosman JH, Koseff JR, Monismith SG, Grover J (2007) A field investigation into the effects of a kelp forest (*Macrocystis pyrifera*) on coastal hydrodynamics and transport. J Geophys Res 112:C02016

Sathyendranath S, Gouveia AD, Shetye SR, Ravindran P, Platt T (1991) Biological control of surface temperature in the Arabian Sea. Nature 349:54–56

Schneider K, Mauser W (1996) Processing and accuracy of Landsat Thematic Mapper data for lake surface temperature measurement. Int J Remote Sens 17:2027–2041

Shell KM, Frouim R, Nakamoto S, Somerville RCJ (2003) Atmospheric response to solar radiation absorbed by phytoplankton. J Geophys Res 108:4445

Smith SD (1980) Wind stress and heat flux over the ocean in gale force winds. J Phys Oceanogr 10:709–726

Son S, Wang M (2015) Diffuse attenuation coefficient of the photosynthetically available radiation K_d(PAR) for global open ocean and coastal waters. Remote Sens Environ 159:250–258

Thomas A, Byrne D, Weatherbee R (2002) Coastal sea surface temperature variability from Landsat infrared data. Remote Sens Environ 81:262–272

Wu Y, Tang CL, Sathyendranath S, Platt T (2007) The impact of bio-optical heating on the properties of the upper ocean: a sensitivity study using a 3-D circulation model for the Labrador Sea. Deep Sea Res II 54:2630–2642

Wu Y, Hannah CG, O'Flaherty-Sproul M, Thupaki P (2017) Representing kelp forests in a tidal circulation model. J Mar Syst 169:73–86

Editorial responsibility: Antony Underwood, Sydney, New South Wales, Australia

Submitted: March 6, 2017; Accepted: August 18, 2017
Proofs received from author(s): September 26, 2017